

Mesh-size Effect Study of Extremely Low Cycle Fatigue Life Prediction for Steel Bridge Piers by Using Different Models

Lan KANG¹ and Hanbin GE²

¹JSPS foreign researcher, Dept. of Civil Eng., Meijo University
(Shiogama-guchi 1-501, Tempaku-ku, Nagoya 468-8502, Japan)
E-mail:connielan@tom.com

²Member of JSCE, Professor, Dept. of Civil Eng., Meijo University
(Shiogama-guchi 1-501, Tempaku-ku, Nagoya 468-8502, Japan)
E-mail:gehanbin@meijo-u.ac.jp

Prediction models based on the Manson-Coffin relation that capture interactions of plastic strain and damage index provide accurate criteria to predict ductile fracture in finite element simulations of structural steel materials and components. Three such models – Tateishi method, Xue method and Ge method – take the effect of extremely low cycle fatigue into account in different ways. Finite element simulations with three different mesh sizes for nine steel bridge piers demonstrate the application of different prediction models to evaluate the ductile crack initiation under cyclic loading in steel structures. While the refined mesh size is 1~2mm, Ge model's results are in good agreement with experimental results. If the refined mesh size is 0.5mm, Tateishi and Xue models may be suitable. This suggests that using appropriate scale finite element model based on different prediction methods is necessary.

Key Words : steel bridge pie, extremely low cycle fatigue (ELCF), mesh size effect, nonlocal damage parameter, ductile crack initiation

1. INTRODUCTION

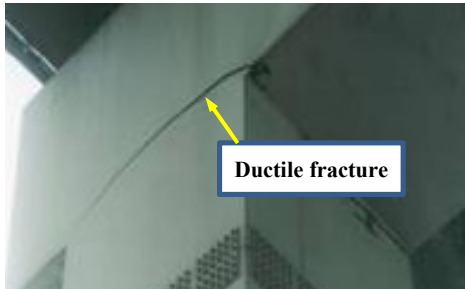
Ductile fracture is one of important failure modes in steel structures, and accurate assessment of ductile fracture is necessary for evaluating structural performance under extreme loads such as earthquakes. A fracture process composed of ductile crack initiation followed by stable crack growth and finally explosive failure in a brittle mode was observed in the damage of steel bridges in Kobe during the 1995 Hyogoken-Nanbu earthquake (as shown in **Fig.1** (a)) and a lot of laboratory tests (as shown in **Fig.1** (b)). Ductile fracture that initiates in fewer than one hundred constant loading cycles is termed as the extremely low cycle fatigue, abbreviated as ELCF [1]. Within this ELCF regime, the failure mechanism is governed by not only fatigue damage but also plastic damage (or sometimes called ductile damage), which is characterized by micro structure deterioration such as micro void nucleation, growth and coalescence, and micro crack initiation and propagation [2]. Ductile fracture was not considered in seismic design

prior to the Kobe earthquake because no similar failure or damage of steel structures has ever been reported in Japan before, and as a result the corresponding evaluation methods were lacking. Nowadays, the necessity to consider ductile fracture (including the ductile crack initiation, propagation and failure) in the phase of seismic design for steel structures, especially for steel bridge piers with thick-walled cross section, has been gradually realized.

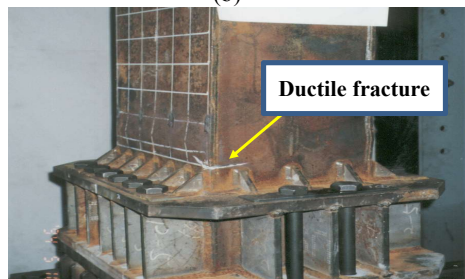
Various prediction models accounting for the combined effects of ductile and fatigue damages are proposed to predict ductile crack initiation life due to large amplitude cyclic straining in structural steels [1-4] and steel structures [5-9]. In which, the ductile crack initiation of steel structures subjected to earthquake-type cyclic loading is evaluated by a local ELCF damage parameter obtained from concentrated plastic strain amplitude. Concerning their applications in large scale steel structures, two key issues still need to be addressed. One is how the concentrated plastic strain is obtained from finite element

analysis. The other is the choice of evaluation model's type and its material constants. For the case of welded steel structures, the material of welded part is not an ideal continuum, including base metal, weld material and heat affected zone (HAZ). The inhomogeneous material and structural discontinuous geometry more easily lead to strain concentration occurring in very small areas. However, the concentrated plastic strain at strain concentration zone is difficult to be accurately and directly measured by strain gauge because of uncertain location of ductile crack initiation. Meanwhile, it will cost too much to accurately predict the local strain amplitude at strain concentration region because of many factors, such as initial defects, complex geometrical details, inhomogeneous material and other uncertain factors. A balance between computation cost and feasibility for large scale structures still needs to be investigated.

This study begins with a brief literature review of various approaches available for prediction of ductile fracture in structural steels, with a discussion of their advantages and characteristics. This is followed by a description of finite element simulations with different mesh sizes, which are conducted to examine the various models. And then comparison and discussion of the test and analytical results are well done to find out the relationship between prediction models and mesh size. Finally, commentary is provided on the results and limitations of different methods.



(a) Ductile fracture of beam-to-column connection in the 1995 Kobe earthquake



(b) Ductile fracture of steel bridge pier in lab

Fig.1 Typical ductile fracture of steel bridge structures

Table 1 Comparison of different modified Manson-Coffin models

Models	Formula and Characteristics
Kuroda model	$\frac{\varepsilon_{p \max}}{\varepsilon_f} + 2N_f \left(\frac{\Delta \varepsilon_p}{\varepsilon_f} \right)^{a'} + \frac{\Delta \varepsilon_p}{C_p} N_f^{k'} = 1$ <p>a', k' and C_p are the material constants, $\varepsilon_{p \max}$ is the maximum tensile plastic strain, ε_f is the corresponding radial strain at fracture caused by monotonic loading.</p> <p>This model consists of damage due to tensile straining, ductility exhaustion during cyclic straining and crack propagation [1].</p>
Tateishi model	$\Delta \varepsilon_p N_f^k = C \cdot C_m$ $C_m = \begin{cases} \left(\frac{\varepsilon_f - \Delta \varepsilon_{\max}}{\varepsilon_f - \varepsilon_{pD}} \right)^k & \text{if } \Delta \varepsilon_{\max} > \varepsilon_{pD} \\ 1.0 & \text{if } \Delta \varepsilon_{\max} \leq \varepsilon_{pD} \end{cases}$ <p>ε_{pD} is the damage strain threshold in pure tension.</p> <p>This modified model introduces the effect of ductile damage into the Manson-Coffin relationship [3].</p>
Xue model	$2N_f \frac{e^{\lambda \left(\frac{\Delta \varepsilon_p}{\varepsilon_0} \right)^m} - 1}{e^\lambda - 1} = 1$ <p>λ, m and ε_0 are the material constants.</p> <p>This model is capable of capturing the cyclic life over the entire span of ELCF to LCF with an additional material parameter to calibrate by introducing an exponential function [2].</p>
Ge model	$D = \sum D_i = C' \sum (\varepsilon_{pr})^m$ <p>where ε_{pr} is the plastic strain range, C' and m are constants determined by steel material test ($C' = 9.69$, $m = 1.86$ in this study).</p> <p>This model is based on the Manson-Coffin law and Miner law, and a damage index is introduced to evaluate ductile crack initiation. It has been successfully applied to ductile crack initiation of steel bridge structures. [6-8].</p>

Notes: $\Delta \varepsilon_p$ and N_f are the plastic strain amplitude and the number of cycles to failure, respectively; k and C are the material constants.

2. REVIEW OF CONVENTIONAL LOCAL DAMAGE MODELS

In the conventional low cycle fatigue (LCF) regime, Manson [10] and Coffin [11] independently proposed the following empirical fatigue life relationship that is referred to as the Manson-Coffin relation:

$$\varepsilon_p \cdot (N_f)^k = C \quad (1)$$

where ε_p and N_f are the plastic strain amplitude and the number of cycles to failure, respectively; k and C are material constants. Equation (1) is represented by a linear relation on the log-log coordinates of ε_p and N_f . Besides, the damage accumulation for LCF under random loading history is based on the Miner's rule [12]. This method assumes that the effect of each cycle is independent, and the damage index D_i is defined as $n_i/N_{f,i}$, where n_i and $N_{f,i}$ are the number of cycles and fatigue life for the i^{th} strain amplitude, respectively. In engineering practice, the cumulative damage index D is equal to zero when there is no damage and is equal to unity when crack initiation occurs. The cumulative damage parameter D is expressed as follows:

$$D = \sum D_i = \sum \left(\frac{n_i}{N_{f,i}} \right) = 1.0 \quad (2)$$

Based on the Manson-Coffin law, some typical prediction models (as named and summarized in **Table 1**) accounting for the combined effects of ductile and fatigue damages have been proposed to establish strain-life relationships that cover both the LCF and ELCF regimes [1-3]. These models consider the effect of ductile damage by modifying the Manson-Coffin relationship. As the strain amplitude increases from the LCF regime to the ELCF regime, the failure mode changes from fatigue fracture to accumulation of ductile damage. In this research, two recent models (Tateishi model and Xue model) are compared and discussed. **Fig.2** shows the fatigue strength curves of plain material, deposited metal and HAZ under constant strain amplitudes for Tateishi model and Xue model.

Tateishi et al. [3] conducted LCF tests on plain steel material and welded materials, such as deposited metal and HAZ, under variable strain amplitude, and based on the constant amplitude test results of different materials, and the corresponding material parameters are obtained, as listed in **Table 2**. Xue [2] proposed a new life prediction model for the entire range of the broad sense of the LCF which covers the ELCF regime. In order to compare the ELCF be-

havior evaluation results using these different models, the authors deduce the material parameters of Xue model (as listed in **Table 3**) based on the test results of small coupons from Tateishi et al. [3]. In this study, the SN curves of HAZ are employed because ductile fractures more easily initiate in the HAZ at the fusion line between the weld and column flange [13].

Furthermore, Ge et al. proposed a method to predict the ductile crack initiation of structural member based on the Manson-Coffin law and Miner law, and a damage index is introduced to evaluate ductile crack initiation [6-8]. The material constants C' and m were attained through nonlinear regression to minimize the square of the results obtained by some cyclic experiments of welded single column specimens, which were applied to a constant cyclic loading. This paper seeks to address these issues by applying three models (Tateishi model, Xue model and Ge model) to evaluate ductile crack initiation of steel bridge piers, and their results are compared and discussed.

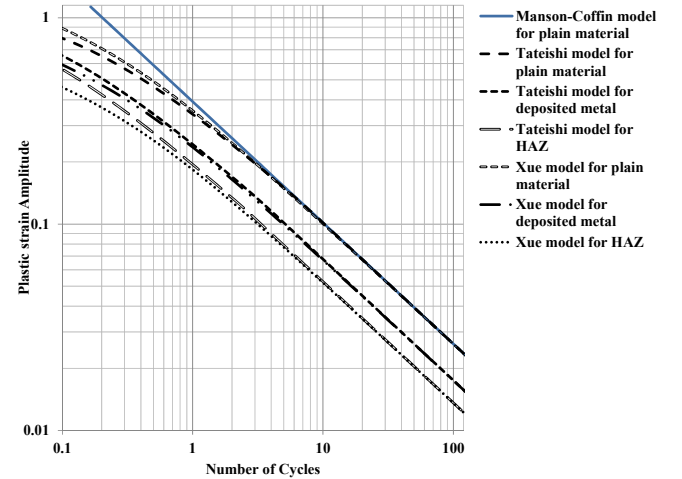


Fig.2 Comparison of different strain-life models

Table 2 Material parameters of Tateishi model

Materials	k	C	ε_f	ε_{pD}
Plain material	0.587	0.392	1.13	0.12
Deposited metal	0.587	0.261	1.14	0.12
HAZ	0.587	0.203	1.14	0.12

Table 3 Material parameters of Xue model based on Tateishi's test results

Materials	λ	m	ε_0
Plain material	0.587	1.704	0.491
Deposited metal	0.587	1.704	0.327
HAZ	0.587	1.704	0.255

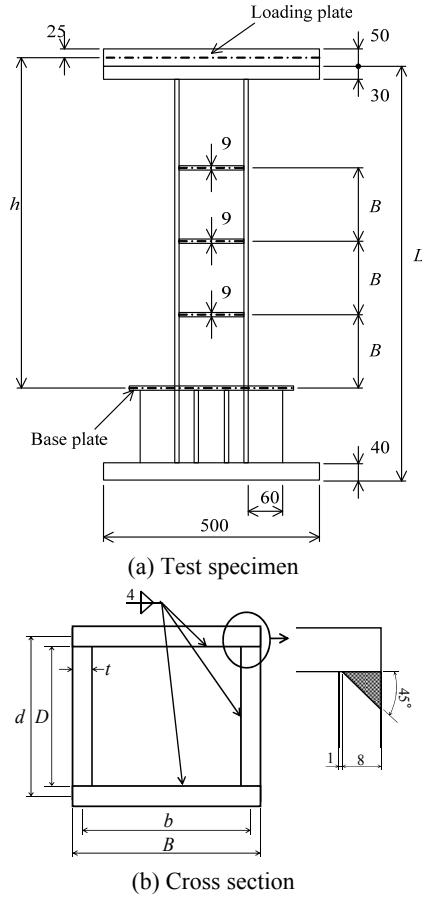


Fig.3 Test specimen and cross section (Unit: mm)

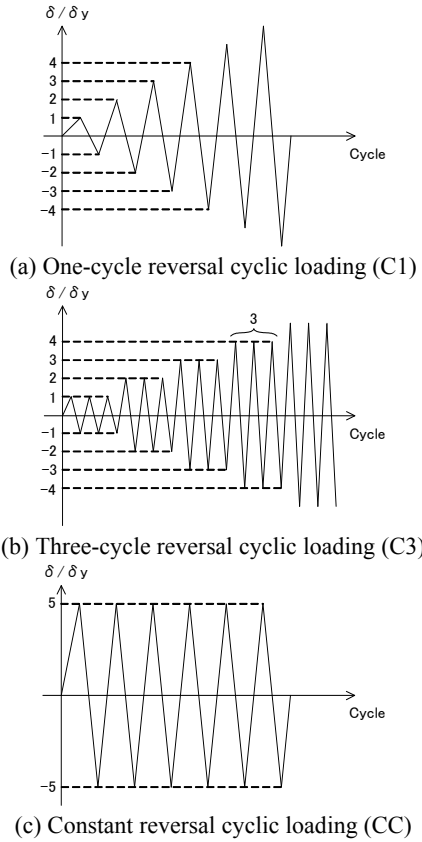


Fig.4 Load patterns

3. MESH DEPENDENCY OF CONVENTIONAL DAMAGE METHODS

(1) Experimental research

To investigate the ductile crack initiation of steel bridge piers under cyclic loading, nine cyclic tests were conducted on steel bridge piers by authors [6]. Effects of various parameters, including loading pattern, width-thickness and slenderness ratios were investigated. Fig.3 illustrated the test specimen and cross section. Geometric dimensions and structural parameters of test specimens with unstiffened box sections [6] were listed in Table 4. Some notations of Table 4 were illustrated in Fig.3. The width-to-thickness ratio parameter and the slenderness ratio parameter are defined as follows [14]:

$$R_f = \frac{b}{t} \sqrt{\frac{12(1-\nu^2)}{4\pi^2 n^2}} \sqrt{\frac{\sigma_y}{E}} \quad (3)$$

$$\bar{\lambda} = \frac{2h}{r} \frac{1}{\pi} \sqrt{\frac{\sigma_y}{E}} \quad (4)$$

where b = flange width measured from plate thickness centerlines, t = flange thickness, h = column height, n = number of subpanels, r = radius of gyration of cross section, E = Young's modulus, ν = Poisson's ratio and σ_y = yield stress.

Three types of lateral loading patterns were employed for experimental specimens, i.e. C1, C3 and CC, respectively, as shown in Fig.4. C1 refers to the one-cycle reversal cyclic loading, which has one cycle at each amplitude and $1\delta_y$ incremental lateral displacement per one cycle. C3 represents the three-cycle reversal cyclic loading, which has three cycles at each amplitude and $1\delta_y$ incremental lateral displacement per three cycles. CC means the constant reversal cyclic loading, which is described as cyclic loading with constant amplitude of $5\delta_y$. Besides, a constant axial compression load ($P=0.1P_y$) was applied at the top of test specimens. All of the tested specimens were made of SM490 (equivalent to ASTM A242), and the material properties of steel material adopted were listed in Table 5.

A summary of the experimental results was listed in Table 6. Based on the test results, some useful findings were obtained. Qualitatively, the ductile crack initiation at the column-to-base weld was experimentally confirmed for all of specimens, and tests all followed a similar sequence of events leading to failure. For different geometrical parameters, the ductile crack initiation appeared before or after the occurrence of local buckling. Subsequent cyclic loads resulted in the ductile cracks growing at the weld toes along web- and flange-direction, and then

propagated into base metal which triggered obvious decrease of strength capacity. A more detailed description of the test results can refer to the reference [6]. A comparison between the test and prediction results is conducted in one following section.

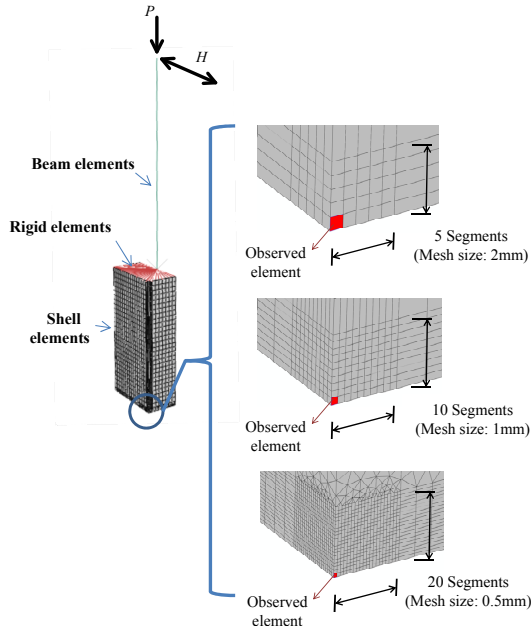


Fig.5 Analytical model

(2) Numerical modeling

In this section, in order to study the ELCF performance of steel bridge piers under earthquake-type cyclic loading, a numerical modeling programme was undertaken. Detailed three-dimensional finite-element models of steel bridge piers were developed. The general finite-element package ABAQUS [15] was used to develop models to replicate the behavior of steel bridge piers tested and the analytical model was shown in Fig.5. Only half of the specimens were required to be modeled because of symmetry, as depicted in Fig.5. Finite element models in this work did not take the detailed weld into account because plastic histories of analytical models with and without weld were very close, and the prediction results of analytical models without weld were safer [7, 8]. The output from the numerical models was used in conjunction with a local strain-based damage prediction method to determine the ductile crack initiation life of steel bridge piers tested.

The 4-node reduced integrated shell element of S4R and the 3-node reduced integrated shell element of S3 were employed for simulating the $2B$ lower part of steel bridge pier specimen, in which B is the flange width. These two elements allow transverse shear deformation and can be used for thick shell or thin shell applications. The upper part of steel bridge pier

specimen was modeled by using the beam-column element of B31 based on Timoshenko beam theory. To accurately simulate local buckling and ductile crack initiation in detail, refined meshes were used only in strain concentration regions, i.e. at the corners of steel bridge piers. Various simulations have been carried out using different mesh sizes (i.e. $2\text{mm}\times 2\text{mm}$, $1\text{mm}\times 1\text{mm}$ and $0.5\text{mm}\times 0.5\text{mm}$) near the corner of piers to investigate the mesh dependency nature of the local evaluations of ELCF performance for the steel bridge piers tested.

A material model capable of simulating cyclic material properties such as the Baushinger effect and expansion of the elastic material range was needed to represent the large plastic strains and load reversals. The nonlinear constitutive law of modified uniaxial two-surface model [16] was adopted in the FE models of the current study. A series of strain-controlled fully reversed cyclic axial tests on coupons cut from the test specimens were carried out to calibrate the cyclic material model. The values of some material parameters were determined in the previous study by [16], and other material parameters were obtained from tension tests of steel coupons made of SM490 in this work, as given in Table 5. The accuracy and feasibility of this material model have been verified to be accurate in predicting the elasto-plastic behavior of steel under cyclic loading in the previous studies [17, 18].

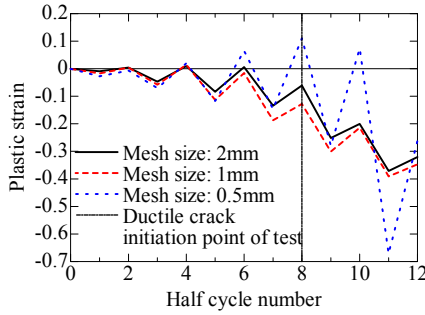
(3) Analytical results

Data from all of the ductile crack initiation life prediction results of three different local evaluation models are summarized in Table 7. Further comparisons of the measured and calculated fatigue lives in Tables 6 and 7 indicate that crack initiation prediction life is related to not only the prediction model but also the finite element mesh size. For the mesh size of $2\text{mm}\times 2\text{mm}$ or $1\text{mm}\times 1\text{mm}$, the ductile crack initiation life prediction by Ge model matches the test result better. On the contrary, for the mesh size of $0.5\text{mm}\times 0.5\text{mm}$, the prediction results of Tateishi model and Xue model show better agreement with test, except for UB35-35-C3P1[490]. It is demonstrated that for the cases of steel bridge piers of this study Tateishi model and Xue model are suitable for the finite element simulation with 0.5mm mesh size, and Ge model is fit for the simulation with $1\text{-}2\text{mm}$ mesh size. But all of the crack initiation prediction life results are sensitive to the mesh size regardless of local evaluation models.

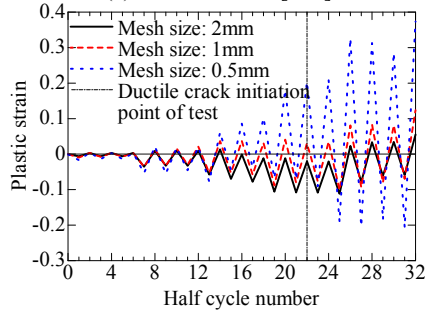
Table 4 Dimensions and structural parameters of tested specimens

Specimens	$R_{f, des}$	$\bar{\lambda}_{des}$	B (mm)	D (mm)	b (mm)	d (mm)	t (mm)	h (mm)	R_f	$\bar{\lambda}$	H_y (N)	δ_y (mm)
UB25-35C1P1[490]	0.25	0.35	112	94	103	103	9.02	570	0.26	0.37	77122	3.94
UB25-35C3P1[490]	0.25	0.35	112	94	103	103	9.02	568	0.26	0.37	77595	3.92
UB25-35CCP1[490]	0.25	0.35	112	94	103	103	9.02	569	0.26	0.37	77585	3.93
UB35-35C1P1[490]	0.35	0.35	152	134	143	143	9.02	769	0.37	0.37	110154	5.18
UB35-35C3P1[490]	0.35	0.35	152	134	143	143	9.02	769	0.37	0.37	110030	5.19
UB35-35CCP1[490]	0.35	0.35	152	134	143	143	9.02	769	0.37	0.37	109671	5.19
UB35-45C1P1[490]	0.35	0.45	152	134	143	143	9.02	999	0.37	0.48	84684	8.44
UB35-45C3P1[490]	0.35	0.45	152	134	143	143	9.02	998	0.37	0.47	84636	8.43
UB35-45CCP1[490]	0.35	0.45	152	134	143	143	9.02	998	0.37	0.47	84636	8.43

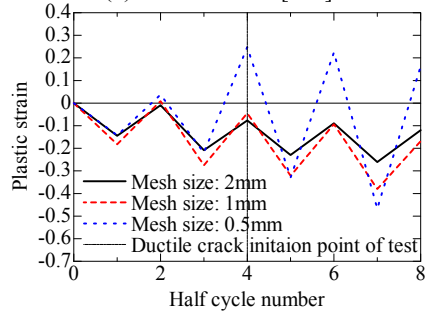
Notes: Notation of a specimen, such as UB $\circ\circ$ - $\Delta\Delta$ C \times P1[490], is explained as follows. UB represents unstiffened box section, $\circ\circ$ refers to the two numerals after decimal point of $R_{f, des}$, and $\Delta\Delta$ refers to that of $\bar{\lambda}_{des}$. $R_{f, des}$ = designed width-to-thickness ratio parameter, $\bar{\lambda}_{des}$ = designed slenderness ratio parameter. C \times indicates cyclic loading patterns. P1 indicates the specimen under an axial compression force. Steel of SM490 is used for series of experiments, which is denoted as [490]. B = flange width, D = web width, t = plate thickness, $b=B-t$, $d=D+t$, h = column height, R_f = real width-to-thickness ratio parameter, $\bar{\lambda}$ = real slenderness ratio parameter, H_y = yield horizontal force, δ_y = yield transverse displacement.



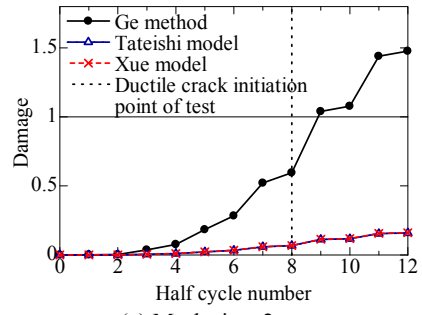
(a) UB35-35C1P1[490]



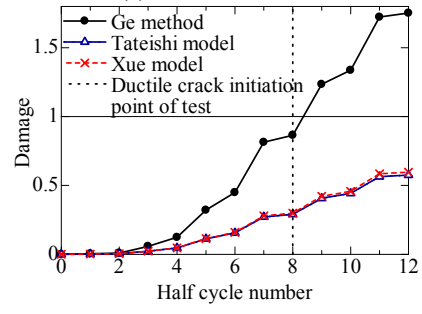
(b) UB35-35C3P1[490]



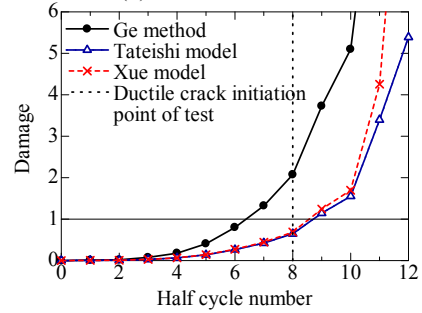
(c) UB35-35CCP1[490]

Fig.6 Plastic strain-half cycle number curves of FE simulations for UB35-35 series with different mesh sizes

(a) Mesh size: 2mm



(b) Mesh size: 1mm



(c) Mesh size: 0.5mm

Fig.7 Damage-half cycle number curves of shell models for UB35-35C1P1[490] using different prediction models

Table 5 Material properties of steel

E (GPa)	ν	σ_y (MPa)	ε_y (%)
199	0.29	380	0.19
ε_{st} (%)	E_{st} (GPa)	σ_u (MPa)	ε_u (%)
2.0	4.20	528	25

Notes: E = Young's modulus, ν = Poisson's ratio, σ_y = yield stress, ε_y = yield strain, ε_{st} = strain at the onset of strain hardening, E_{st} = initial strain hardening modulus, σ_u = ultimate stress (tensile strength), ε_u = ultimate strain.

Table 6 Ductile crack initiation and local buckling occurrence results of test

Specimens	Ductile crack initiation	Local buckling occurrence	$n_{hc,lb} - n_{hc,dc}$
	$n_{hc,dc}$	$n_{hc,lb}$	
UB25-35C1P1[490]	12	/	/
UB25-35C3P1[490]	26	/	/
UB25-35CCP1[490]	6	/	/
UB35-35C1P1[490]	8	11	3
UB35-35C3P1[490]	22	25	3
UB35-35CCP1[490]	4	7	3
UB35-45C1P1[490]	8	9	1
UB35-45C3P1[490]	18	19	1
UB35-45CCP1[490]	4	3	-1

Notes: $n_{hc,dc}$ = half cycle number of ductile crack initiation from test; $n_{hc,lb}$ = half cycle number of local buckling occurrence from test; / means that no local buckling occurred during test.

(4) Plastic strain and damage accumulation

Taking UB35-35 series as example, **Fig.6** illustrates the plastic strain-half cycle number curves for UB35-35C1P1[490], UB35-35C3P1[490] and UB35-35CCP1[490], respectively. As shown in **Fig. 5**, the element near the corner of pier, i.e. damage-critical location, was observed in this study. It is illustrated in **Fig.6** that the plastic strain at the corner region of piers is sensitive to mesh size, and increases in compression with increase of half cycle number regardless of loading patterns. The plastic strain histories of finite element simulations with 2mm and 1mm mesh sizes are relatively close. It is obvious that the plastic strain more obviously and easily concentrates while using analytical model with finer mesh, especially in the simulation with 0.5mm mesh size. The damage index is directly related to the plastic strain history. Because of the localization of plastic strain history, the damage index of steel structure has the property of localization. Before the ductile crack initiation, the mesh size effect is very obvious. This implies that the mesh size has great effect on the crack initiation life prediction.

Taking UB35-35C1P1[490] as example, the plots in **Fig.7** illustrate how the damage index D increases as cyclic load processing, and they are obtained from finite element simulations with different mesh sizes using different prediction models. Because the Tateishi model and Xue model have the similar SN curves as shown in **Fig.2**, the damage prediction result of the Tateishi model is nearly the same as that of the Xue model. It is observed from **Fig.7** that the damage evolutions of different models are also sensitive to the mesh size with different degrees. Ge model's results are safer than another two models. In other words, Tateishi and Xue models are effective when the strain concentration must be enough large.

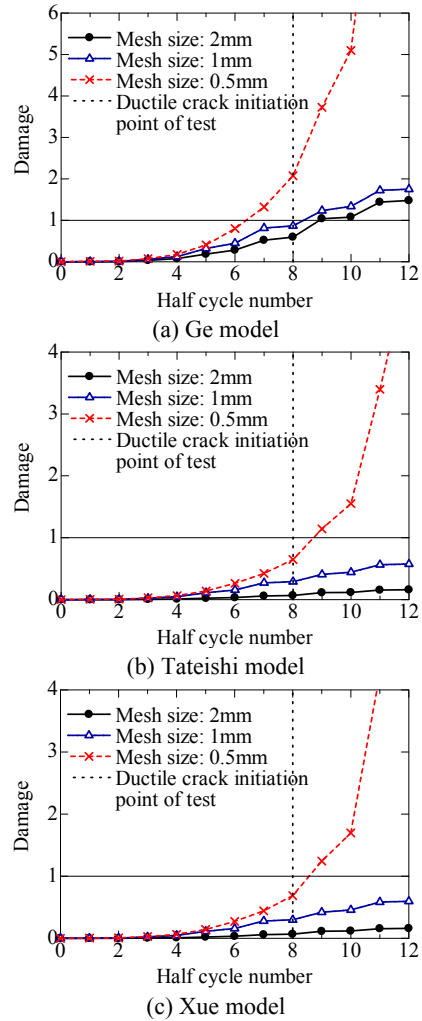
**Fig.8** Damage-half cycle number curves of shell models for UB35-35C1P1[490] with different mesh sizes

Fig.8 presents the damage-half cycle number curves of finite element models with different mesh sizes. For all of prediction models, the cumulative damage increases with finer mesh. The material parameters of Tateishi model and Xue model served as the basis for evaluating the ductile crack initiation for cyclically strained structural steels come from the tests of small-scale material specimens or small

coupons. In the fatigue test of steel materials, **Fig.2** shows the crack initiation life of the steel material, which was defined as the number of cycles when the fatigue crack was found on the specimen surface by digital microscope. At that time, the fatigue crack was about 0.5mm in surface length [19]. But for the ductile fracture test of structural members, the ductile crack was detected by eyes, as well as digital camera. And the crack was about 1-2mm in surface length at that time [6]. For these ductile crack scale reasons, different results are obtained using different prediction models.

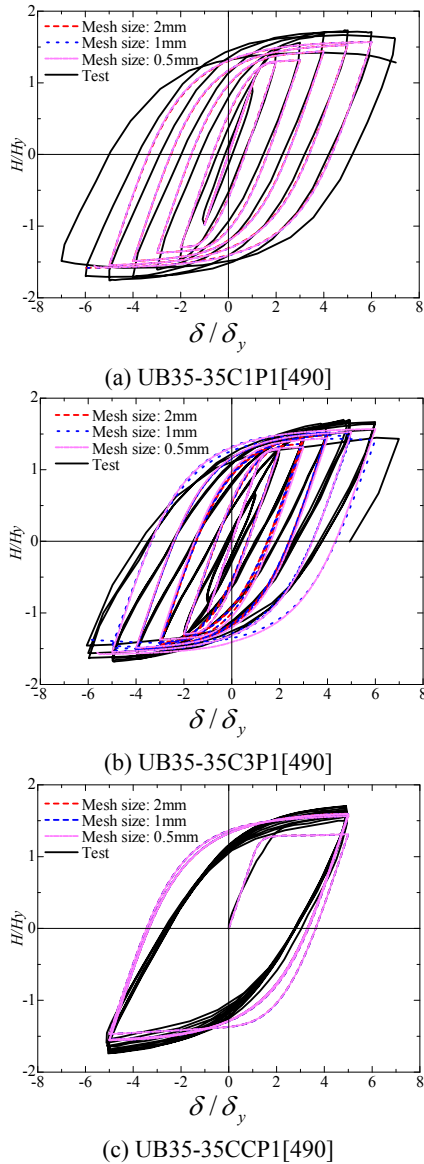


Fig.9 Lateral load-displacement hysteretic curves for UB35-35 series

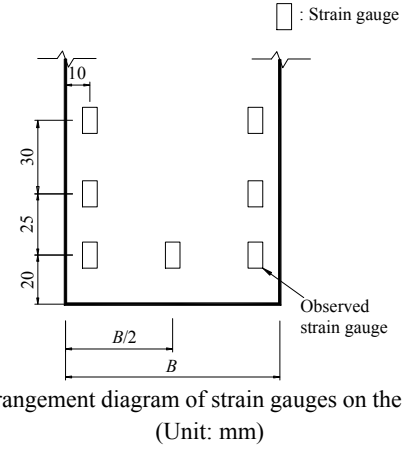


Fig.10 Arrangement diagram of strain gauges on the flange plate (Unit: mm)

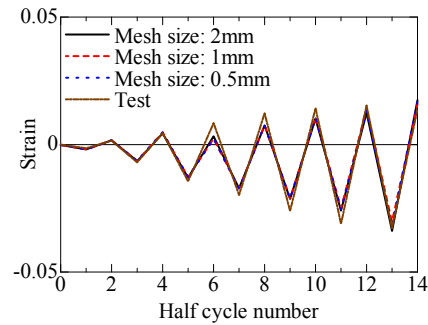


Fig.11 Strain-half cycle number curves of the measured location far away from strain concentration zone (UB25-35C1P1[490])

(5) Hysteretic curves and strain history far away from strain concentration region

Fig.9 shows that the lateral load-displacement hysteretic curves obtained from both test and analysis, where the horizontal load and the horizontal displacement are divided by H_y and δ_y , respectively, to be dimensionless. It is observed that the results from the FEM analysis generally agree fairly well with the results of structural experiments. And the mesh size has no effect on the lateral load-displacement curves from analysis.

In order to verify the proposed evaluation method, strains were also measured using the conventional gauge method during test. The arrangement diagram of strain gauges on the flange is illustrated in **Fig.10**, in which the observed gauge is indicated. Taking UB25-35C1P1[490] as example, **Fig.11** shows the measured strain history 20mm away from strain concentration region, and the close agreement in the strain histories of test and analysis is encouraging. Same to the lateral load-displacement hysteretic curve, the different finite element sizes almost have no obvious effect on the strain history far away from the strain concentration zone. From the test and analytical results, we can conclude that the results of finite element analysis in this study are reliable and the ductile crack occurs in relatively local zone.

Table 7 Ductile crack prediction results using different models

Models	UB25-35C1P1[490]			UB25-35C3P1[490]			UB25-35CCP1[490]		
	2mm	1mm	0.5mm	2mm	1mm	0.5mm	2mm	1mm	0.5mm
Ge model	11	9	8	23	19	15	5	3	3
Tateishi model	/	14	10	/	27	20	/	8	6
Xue model	/	14	10	/	27	17	/	8	6
Different models	UB35-35C1P1[490]			UB35-35C3P1[490]			UB35-35CCP1[490]		
	2mm	1mm	0.5mm	2mm	1mm	0.5mm	2mm	1mm	0.5mm
Ge model	9	9	7	20	20	16	4	3	2
Tateishi model	/	/	9	/	28	21	/	5	4
Xue model	/	/	9	/	28	21	/	5	4
Different models	UB35-45C1P1[490]			UB35-45C3P1[490]			UB35-45CCP1[490]		
	2mm	1mm	0.5mm	2mm	1mm	0.5mm	2mm	1mm	0.5mm
Ge model	11	9	7	21	15	14	4	3	2
Tateishi model	/	/	9	/	22	17	/	7	4
Xue model	/	/	9	/	21	17	/	6	4

Notes: Gray section means that the quantity is the fittest prediction result compared to test result as listed in Table 6. / means that no ductile crack initiation occurs using this model under 1.5 times of half cycle number of ductile crack initiation from test.

4. CONCLUSIONS

This paper applies various prediction methods to evaluate the ductile crack initiation of steel bridge piers. These approaches include Tateishi model, Xue model and Ge method, and they are based on the Manson-Coffin law and the Miner's rule. These methods take the effect of extremely low cycle fatigue into account in different ways. The applications of various methods are examined through nine structural experiments on steel bridge piers and finite element simulations with different mesh sizes are employed. Further comparison and discussion of the ductile fracture initiation predicted by the various methods and those observed in the experiments reveal several interesting points. To summarize these briefly, predicting ELCF fracture with various prediction models involves monitoring the plastic strain histories over the appropriate scale finite element model.

From the view of finite element mesh size, the prediction results of models with different mesh sizes are different. The ductile fatigue life decreases with decrease of the mesh size. And the results of simulation with 2mm mesh size are close to the results of simulation with 1mm mesh size. But the results of simulation with 0.5mm mesh size is far from simulations with another two mesh sizes because the plastic strain more obviously concentrates while using analytical model with finer mesh size.

While the refined mesh size of simulation is 0.5mm, the prediction results of Tateishi and Xue

models show much greater promise in predicting ductile crack initiation accurately. As the mesh size of simulation is 1mm or 2mm, over-estimation of fatigue life is obtained. On the contrary, if the mesh size is 1mm or 2mm, the results of Ge method show better agreement with the test results. When the mesh size is 0.5mm, Ge method results in conservative estimates of ductile crack initiation. This suggests that using appropriate finite element mesh size based on various prediction methods is necessary.

Tateishi model, Xue model and Ge method are observed to be reasonably accurate tools to predict ductile crack initiation of steel components. The parameters of Tateishi and Xue models come from small material tests, and relatively finer mesh size and more computational time are needed. The two models are sensitive to the mesh size. The parameters of Ge method take the effects of finite element scale, ductile damage and weld into account, it can be applied to relatively coarse mesh simulation and more than 7/8 computational time can be saved than another two prediction models.

ACKNOWLEDGMENTS: The study is supported in part by grants from 1) the JSPS Grants-in-Aid for Scientific Research (C) (No. 24560588), and 2) the Advanced Research Center for Natural Disaster Risk Reduction, Meijo University, which supported by Ministry of Education, Culture, Sports, Science and Technology (MEXT), Japan. Besides, the first author is thankful for financial support from the JSPS postdoctoral fellowship program for foreign researchers (Grant No. 12067).

REFERENCES

- 1) Kuroda M.: Extremely low cycle fatigue life prediction based on a new cumulative fatigue damage model, *International Journal of Fatigue*, Vol. 24, pp. 699-703, 2001.
- 2) Xue L.: A unified expression for low cycle fatigue and extremely low cycle fatigue and its implication for monotonic loading, *International Journal of Fatigue*, Vol. 30, pp. 1691-8, 2008.
- 3) Tateishi K., Hanji T. and Minami K.: A prediction model for extremely low cycle fatigue strength of structural steel, *International Journal of Fatigue*, Vol. 29, pp. 887-96, 2007.
- 4) Nip K. H., Gardner L., Davies C. M. and Elghazouli A. Y.: Extremely low cycle fatigue tests on structural carbon steel and stainless steel, *Journal of Constructional Steel Research*, Vol. 66, pp. 96-110, 2010.
- 5) Hanji T. and Tateishi K.: A proposal on low cycle fatigue strength curve for base joints of steel bridge pier, *Steel Construction Engineering, JSSC*, Vol. 16, pp. 21-30, 2009 (in Japanese).
- 6) Ge H. B. and Tsumura Y.: Experimental and analytical study on the evaluation of ductile crack initiation in steel bridge piers, *Journal of Structural Engineering JSCE*, Vol. 55A, pp. 605-16, 2009 (in Japanese).
- 7) Ge H. B., Fujie W. and Tajima R.: Experimental verification of an evaluation method for predicting the ductile crack initiation in steel structures, *Journal of Structural Engineering JSCE*, Vol. 55A, pp. 617-28, 2009 (in Japanese).
- 8) Ge H. B. and Kang L.: A damage index based evaluation method for predicting the ductile crack initiation in steel structures, *Journal of Earthquake Engineering*, Vol. 16, pp. 623-43, 2012.
- 9) Kuwamura H.: Classification of material and welding in fracture consideration of seismic steel frames, *Engineering Structures*, Vol. 25, pp. 547-63, 2003.
- 10) Manson S. Behaviour of materials under conditions of thermal stress. *Cleveland: Lewis Flight Propulsion Laboratory*; 1954.
- 11) Coffin Jr L. F.: A study of the effects of cyclic thermal stresses on a ductile metal, *Transactions of the American Society of Mechanical Engineers*, Vol. 76, pp. 931-50, 1954.
- 12) Miner M. A.: Cumulative damage in fatigue, *Journal of Applied Mechanics*, Vol. 12, pp. A159-A64, 1945.
- 13) Myers A. T., Kanvinde A. M., Deierlein G. G. and Fell B. V.: Effect of weld details on the ductility of steel column baseplate connections, *Journal of Constructional Steel Research*, Vol. 65, pp. 1366-73, 2009.
- 14) Ge H. B., Kawahito M. and Ohashi M.: Experimental study on ductile crack initiation and its propagation in steel bridge piers of thick-walled box sections, *Journal of Structural Engineering JSCE*, Vol. 53A, pp. 493-502, 2007 (in Japanese).
- 15) ABAQUS. ABAQUS/Analysis User's Manual-version 6.9: *ABAQUS, Inc.*: Pawtucket, Rhode Island; 2011.
- 16) Shen C., Mamaghani I. H. P., Mizuno E. and Usami T.: Cyclic behavior of structural steels. II: Theory, *Journal of Engineering Mechanics ASCE*, Vol. 121, pp. 1165-72, 1995.
- 17) Ge H. B., Gao S. B. and Usami T.: Stiffened steel box columns. Part 1: Cyclic behaviour, *Earthquake Engineering & Structural Dynamics*, Vol. 29, pp. 1691-706, 2000.
- 18) Usami T., Gao S. B. and Ge H. B.: Stiffened steel box columns. Part 2: Ductility evaluation, *Earthquake Engineering & Structural Dynamics*, Vol. 29, pp. 1707-22, 2000.
- 19) Tateishi K. and Hanji T.: Low cycle fatigue strength of butt-welded steel joint by means of new testing system with image technique, *International Journal of Fatigue*, Vol. 26, pp. 1349-56, 2004.